PHYSICAL REVIEW A **93**, 042109 (2016)

Coherent exciton dynamics in a dissipative environment maintained by an off-resonant vibrational mode

E. K. Levi,[1,*] E. K. Irish,[2] and B. W. Lovett[1,†]
[1]*SUPA, School of Physics and Astronomy, University of St. Andrews, St. Andrews, Fife KY16 9SS, United Kingdom*
[2]*School of Physics and Astronomy, University of Southampton, Southampton SO17 1BJ, United Kingdom*
(Received 4 February 2016; published 14 April 2016)

The interplay between an open quantum system and its environment can lead to both coherent and incoherent behavior. We explore the extent to which strong coupling to a single bosonic mode can alter the coherence properties of a two-level system in a structured environment. This mode is treated exactly, with the rest of the environment comprising a Markovian bath of bosonic modes. The strength of the coupling between the two-level system and the single mode is varied for a variety of forms for the bath spectral density in order to assess whether the coherent dynamics of the two-level system are modified. We find a clear renormalization of the site population oscillation frequency that causes an altered interaction with the bath. This leads to enhanced or reduced coherent behavior of the two-level system, depending on the form of the spectral density function. We present an intuitive interpretation, based on an analytical model, to explain the behavior.

DOI: 10.1103/PhysRevA.93.042109

I. INTRODUCTION

Open quantum systems have been an active area of research for decades, but only recently have measurements been able to probe the dynamical effects of a coupled environment in detail [1–4]. The environment has historically been thought to lead to deleterious decoherence of the open system, but it is now accepted that the role of the environment can be much more subtle than this. In particular, the importance of structured environments in the dynamics and coherence of open quantum systems is now beginning to be recognized. For example, a series of recent theoretical [5–12] and experimental [13–16] studies has provided strong evidence that strongly coupled discrete molecular vibrations play a significant role in the speed, efficiency, and quantum coherence of energy transfer in photosynthetic and other molecular systems. In a different context, the high degree of control and precision possible in artificial nanosystems has enabled experimental measurement and engineering of noise spectral densities in condensed matter systems. Studies on micromechanical resonators have revealed a strongly subohmic spectral density (SD) [17]; in another series of experiments, a superconducting flux qubit was used to probe the SD of a microwave transmission line, which could be tuned between ohmic and Lorentzian forms using partial reflectors [18].

To mathematically model an open quantum system exactly one must fully capture the dynamics of the environment, and this is usually an impossible task: its Hilbert space is vast. Necessarily the environment must be treated using various approximations. One common description employs the Markov approximation, meaning that future behavior depends only on the current state, with no memory of preceding interaction [19]. Markovian environments are generally straightforward to simulate since the dissipative system dynamics are characterized by a set of constant decay rates, which are found from the easily obtained SD function. When system-environment correlations decay more slowly the approximation becomes invalid and non-Markovian approaches are needed. There exists a spectrum of techniques for dealing with non-Markovianity to varying degrees including master equations [19], quasiadiabatic path integrals [20,21], quantum Monte Carlo techniques [22,23], hierarchy equations of motion [24], multilayer [25] and multiconfiguration time-dependent Hartree theory [26], time-dependent numerical [27] and density matrix [28] renormalization-group approaches, time-dependent variational matrix product states [29], and Dirac-Frenkel methods [30,31].

In this paper we introduce non-Markovianity straightforwardly by including part of the "environment" in the open system; that is, our open system consists of both the two-level system (TLS) whose dynamics we want to model and a single oscillator mode (SM). The rest of the (bosonic) bath is assumed to be weakly coupled to the open system and to be Markovian. Thus we are able to accurately study a structured environment consisting of a continuous background of modes with a strongly coupled single mode at one particular frequency. This framework maps to a host of physical situations: for example, a multisite chromophore array in a protein bath typical of photosynthesis, where local protein vibrational modes interact strongly with excitons [32], and superconducting qubits coupled to nanomechanical oscillators or microwaves in resonators [33,34]. We present our work in the context of a two-site energy transfer system, or dimer, in the two-state subspace of single exciton levels.

A single-mode representation of certain strong features of a structured environmental coupling has been studied previously [35–39], and symmetries have been exploited to reduce the complexity of the resulting system description [40,41]. However, the particular configuration of the TLS-SM-bath system investigated here is not represented in these earlier studies, in which the SM either couples to, or is not distinguished from, the bath. A similar model incorporating a single common mode was used to demonstrate enhanced coherence in the excitonic dynamics of an asymmetric dimer with individual Markovian baths for each dimer site [42]. In contrast to our model, a polaron transform was used to approximately treat

*ekl3@st-andrews.ac.uk
†bwl4@st-andrews.ac.uk

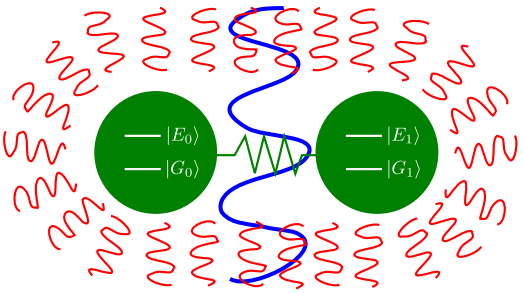

FIG. 1. Schematic of the model given in Eq. (1). The symmetric dimer is composed of two identical sites with a Förster-type interaction between them (green circles). This is linearly coupled to a Markovian bosonic environment of oscillators (short red wavy lines). One bosonic mode of the environment (long blue wavy line) is assumed to be much more strongly coupled to the dimer than the others and is, therefore, considered part of the system that must be treated exactly.

non-Markovian effects. A further asymmetric dimer model explores the role of vibrational modes on the electronic coherence in photosynthetic protein complexes [8].

In the next section we specify our TLS-SM-bath system, deriving a weak-coupling master equation to describe its dynamics. In Sec. III we present numerical results for the dynamics of the TLS across a broad range of parameters. We analyze and discuss these findings in Sec. IV and propose an intuitive and analytical interpretation of the complex dynamics observed. We conclude in Sec. V.

II. MODEL

The symmetric dimer consists of two identical sites, labeled "0" and "1," each with a ground $|G\rangle$ and a single-exciton excited state $|E\rangle$. Both sites are coupled to a single vibrational mode and a bosonic Markovian environment as displayed in Fig. 1. The total Hamiltonian may be written

$$H_{\text{Full}} = H_{\text{TLS}} + H_{\text{SM}} + H_{\text{TLS-SM}} + H_{\text{B}} + H_{\text{TLS-B}}. \quad (1)$$

The electronic part of the dimer Hamiltonian is

$$H_{\text{TLS}} = \varepsilon(|E_0\rangle\langle E_0| + |E_1\rangle\langle E_1|) - J(|E_0G_1\rangle\langle G_0E_1| + \text{H.c.}), \quad (2)$$

where the excitation energy at each dimer site is ε and the Förster coupling between them is J. The terms involving the vibrational mode are

$$H_{\text{SM}} = \Omega\hat{a}^\dagger\hat{a}, \quad (3)$$

$$H_{\text{TLS-SM}} = -(g_0|E_0\rangle\langle E_0| + g_1|E_1\rangle\langle E_1|)(\hat{a}^\dagger + \hat{a}), \quad (4)$$

where the vibrational mode has frequency Ω and creation and annihilation operators $\hat{a}^\dagger$ and $\hat{a}$ and couples to each site with strength $g_0 = -g_1 = g$. The terms involving the rest of the bosonic bath are

$$H_{\text{B}} = \sum_{\mathbf{q}} \omega_{\mathbf{q}}\hat{b}_{\mathbf{q}}^\dagger\hat{b}_{\mathbf{q}}, \quad (5)$$

$$H_{\text{TLS-B}} = -\sum_{\mathbf{q}}(h_{\mathbf{q},0}|E_0\rangle\langle E_0| + h_{\mathbf{q},1}|E_1\rangle\langle E_1|)(\hat{b}_{\mathbf{q}}^\dagger + \hat{b}_{\mathbf{q}}). \quad (6)$$

This environment is comprised of harmonic modes of wave vector $\mathbf{q}$ with frequencies $\omega_{\mathbf{q}}$, creation and annihilation operators $\hat{b}_{\mathbf{q}}^\dagger$ and $\hat{b}_{\mathbf{q}}$, and coupling strengths of $h_{\mathbf{q},0} = -h_{\mathbf{q},1} = h_{\mathbf{q}}$.

The Hamiltonian in Eq. (1) consists of three uncoupled subspaces with basis vectors $\{|G_0G_1\rangle\}$, $\{|E_0E_1\rangle\}$, and $\{|E_0G_1\rangle, |G_0E_1\rangle\}$. In order to study energy transfer dynamics we may focus only on the last: the two-dimensional single excitation subspace. To simplify notation we then define $|0\rangle = |E_0, G_1\rangle$ and $|1\rangle = |G_0, E_1\rangle$.

In this subspace our Hamiltonian becomes

$$H_{\text{F}} = -J\hat{X} - \hat{Z}g(\hat{a}^\dagger + \hat{a}) - \hat{Z}\sum_{\mathbf{q}} h_{\mathbf{q}}(\hat{b}_{\mathbf{q}}^\dagger + \hat{b}_{\mathbf{q}}) + \Omega\hat{n} + \sum_{\mathbf{q}} \omega_{\mathbf{q}}\hat{n}_{\mathbf{q}}, \quad (7)$$

where $\hat{n} = \hat{a}^\dagger\hat{a}$ and $\hat{n}_{\mathbf{q}} = \hat{b}_{\mathbf{q}}^\dagger\hat{b}_{\mathbf{q}}$ are the number operators for the SM and the $\mathbf{q}$th bath mode. We have now reformulated the problem into that of a single TLS interacting with the SM and environment where the site-basis Pauli matrices are $\hat{Z} = |0\rangle\langle 0| - |1\rangle\langle 1|$ and $\hat{X} = |0\rangle\langle 1| + |1\rangle\langle 0|$. The form in Eq. (7) is that of a modified spin-boson Hamiltonian; the spin-boson model is one of the most utilized and investigated descriptions of open quantum system behavior [43–48]. While not exactly solvable (except in special cases) it contains information about the interplay between a two-level "spin" system and a harmonic bath. Our model differs from the standard spin-boson model by the addition of the SM to the part of the system that is treated exactly. Both the SM and the bath couple to the TLS via a linear displacement with respect to the site basis.

Disregarding the bath for now, Eq. (7) becomes

$$H = -J\hat{X} - \hat{Z}g(\hat{a}^\dagger + \hat{a}) + \Omega\hat{n}. \quad (8)$$

This is amenable to the Fulton-Gouterman transformation (FGT), which can simplify its solution. First introduced in 1961 [49] and later refined and extended [50], the FGT exploits the parity symmetries of the system to diagonalize the Hamiltonian in the TLS subspace. It is a unitary transformation, and although there are various equivalent forms in the literature we use [51]

$$U = \frac{1}{\sqrt{2}}[|0\rangle\langle 0| - |1\rangle\langle 0| + \hat{P}(|0\rangle\langle 1| + |1\rangle\langle 1|)]. \quad (9)$$

The oscillator parity operator, $\hat{P} = (-1)^{\hat{n}}$, obeys the anticommutation relations

$$\{\hat{P}, \hat{a}\} = \{\hat{P}, \hat{a}^\dagger\} = 0. \quad (10)$$

The function of the FGT is to isolate states of the same parity, which do not couple to states of opposite parity. As shown in Appendix A, the FGT is equivalent to a change of basis and state reordering. Application of the FGT to Eq. (8) yields

$$\tilde{H} = UHU^\dagger = \frac{H^+}{2}|0\rangle\langle 0| + \frac{H^-}{2}|1\rangle\langle 1|, \quad (11)$$

thus creating subspace Hamiltonians of conserved parity:

$$H^\pm = \Omega\hat{n} - g(\hat{a}^\dagger + \hat{a}) \mp J\hat{P}. \quad (12)$$

The eigenstates of these transformed Hamiltonians, expanded in the site basis, are

$$|\psi_k^{\pm}\rangle = \frac{1}{\sqrt{2}}[\pm|0\rangle + \hat{P}|1\rangle]|\phi_k^{\pm}\rangle, \tag{13}$$

where $|\phi_k^{\pm}\rangle$ are the eigenstates of the excitation parity subspace Hamiltonians. To clarify, the Schrödinger equations are then $H^{\pm}|\phi_k^{\pm}\rangle = E_k^{\pm}|\phi_k^{\pm}\rangle$ and $\tilde{H}|\psi_k^{\pm}\rangle = E_k^{\pm}|\psi_k^{\pm}\rangle$.

Using a Fock basis for the SM and $|\pm\rangle \equiv (|0\rangle \pm |1\rangle)/\sqrt{2}$ for the TLS, the FGT shows that the Hamiltonian takes a tridiagonal form that can be diagonalized efficiently. It is of course necessary to truncate the expansion of the SM, but for all calculations we ensure that simulations are numerically converged. With this in mind we refer to our treatment of this TLS-SM system as exact.

We now reintroduce the bath. In the $|\pm\rangle$ basis, the Hamiltonian in Eq. (8) becomes

$$H_S = -J\hat{\sigma}_z - \hat{\sigma}_x g(\hat{a}^{\dagger} + \hat{a}) + \Omega\hat{n}, \tag{14}$$

where now $\hat{\sigma}_z = |+\rangle\langle+| - |-\rangle\langle-|$, $\hat{\sigma}_x = |+\rangle\langle-| + |-\rangle\langle+|$, and we have introduced the subscript "S" to denote the system of TLS and SM. The Hamiltonian describing the interacting system and bath is then

$$H_F = H_S + \sum_{\mathbf{q}} \omega_{\mathbf{q}}\hat{n}_{\mathbf{q}} + \hat{\sigma}_x \sum_{\mathbf{q}} h_{\mathbf{q}}(\hat{b}_{\mathbf{q}}^{\dagger} + \hat{b}_{\mathbf{q}}). \tag{15}$$

From this Hamiltonian we can derive a Markovian master equation, assuming that the TLS-SM system is coupled only weakly to the environmental oscillators. We have found a convenient form for the eigenstates of H_S which simplifies the master equation derivation if we describe the $\hat{\sigma}_x$ interaction in this basis; this is shown in Appendix B.

The general form of the master equation following the Born-Markov approximation is, in the interaction picture,

$$\frac{d\rho_S(t)}{dt} = -\int_0^{\infty} ds\ \mathrm{Tr}_B\{[H_I(t),[H_I(t-s),\rho_S(t)\otimes\rho_B]]\}, \tag{16}$$

which describes the dynamics of a reduced system density matrix, $\rho_S(t)$. ρ_B is the bath density matrix, assumed to represent a thermal state at all times, and $H_I(t)$ is the interaction-picture interaction Hamiltonian [19]. For our problem this becomes

$$\begin{aligned}\frac{d\rho_S(t)}{dt} = \sum_{k,k'}\{&[\Gamma(-\Lambda_{kk'}) + \Gamma'(\Lambda_{kk'})] \\ &\times [2\hat{\xi}_{k'k}^{-}\rho_S(t)\hat{\xi}_{kk'}^{+} - \hat{\xi}_{kk'}^{+}\hat{\xi}_{k'k}^{-}\rho_S(t) - \hat{\xi}_{k'k}^{-}\hat{\xi}_{kk'}^{+}\rho_S(t)] \\ &+ [\Gamma(\Lambda_{kk'}) + \Gamma'(-\Lambda_{kk'})] \\ &\times [2\hat{\xi}_{kk'}^{+}\rho_S(t)\hat{\xi}_{k'k}^{-} - \hat{\xi}_{k'k}^{-}\hat{\xi}_{kk'}^{+}\rho_S(t) - \hat{\xi}_{kk'}^{+}\hat{\xi}_{k'k}^{-}\rho_S(t)]\}.\end{aligned} \tag{17}$$

The $\hat{\xi}_{ij}^{\pm}$ operators are Lindblad operators describing transitions between the FGT subspaces, from eigenstate j to eigenstate i; these are defined explicitly in Eqs. (B18) and (B19). The transition rates are governed by Γ and Γ', which are defined in Eqs. (C11)–(C14); these rely on bath operator correlators and, by extension, the SD $\chi(\omega) = \sum_{\mathbf{q}} |h_{\mathbf{q}}|^2\,\delta(\omega - \omega_{\mathbf{q}})$, and they are derived in Appendix C. $\Lambda_{kk'}$ is the difference between FGT subspace eigenvalues, $E_k^{+} - E_{k'}^{-}$. We used numerical simulations [52] to solve Eq. (17), the full derivation of which is given in Appendix C.

We use the SD

$$\chi_m(\omega) = A_m\omega^m e^{-\omega^2/\omega_{m,c}^2}, \tag{18}$$

where varying m moves between an ohmic ($m = 1$) and a superohmic ($m > 1$) form. The Gaussian cutoff in this definition ensures that $\chi \to 0$ for $\omega \gg \omega_{m,c}$, the cutoff frequency, meaning that high-frequency modes do not contribute to the dynamics. We impose $\chi(\omega) = 0$ for $\omega \leqslant 0$ and we introduce ω_p to denote the frequency at the peak of the SD, which is related to m and $\omega_{m,c}$. For comparison we also sometimes use a Lorentzian-like form for the SD,

$$\chi_L(\omega) = \frac{A_L\omega W^2}{(\omega - \omega_{L,c})^2 + W^2}, \tag{19}$$

where W is the half-width at half-maximum and $\omega_{L,c}$ is determined by fixing ω_p. The normalization factors, A_m and A_L, in Eqs. (18) and (19) are related to a property of the bath known as the reorganization energy:

$$\lambda = \int_0^{\infty} d\omega \frac{\chi(\omega)}{\omega}. \tag{20}$$

This quantifies the energy associated with the bath as it interacts with the TLS [53]. Defining a fixed value of λ ensures fair SD comparisons in simulations; normalization factors can then be calculated using Eq. (20). We also fix ω_p to ensure peak alignment during comparisons.

We have studied dynamics for $m = 1, 3, 5, 7$ and Lorentzian spectral densities; for reference these are shown (for a constant λ and ω_p) in Fig. 2. Ohmic spectral densities are frequently used for low temperatures or for surface-surface

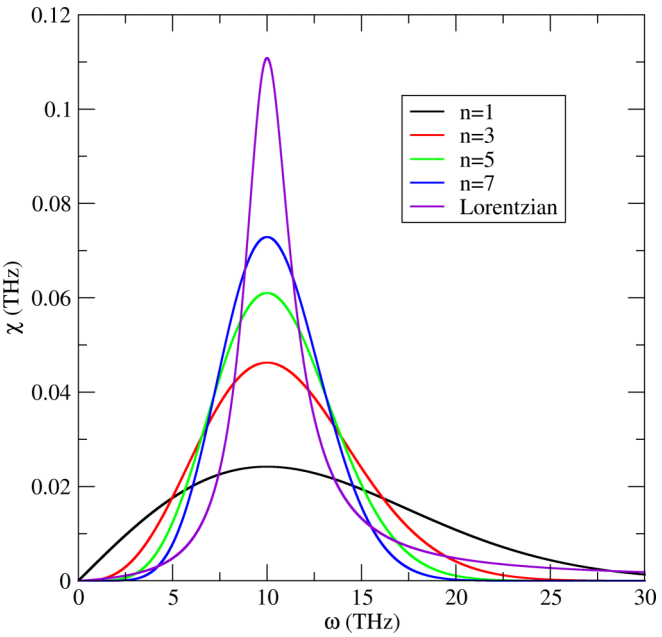

FIG. 2. Comparative plot of the five spectral densities considered here, with $\lambda = 0.05$ THz and $\omega_p = 10$ THz. The ohmic SD is given by $m = 1$, while $m = 3$, 5, and 7 represent increasingly peaked superohmic spectral densities. The Lorentzian SD has width $W = 1.5$ THz.

tunneling problems, while superohmic descriptions apply well to bulk phonon baths [43,54]. The Lorentzian SD in Fig. 2 is far more peaked than the ohmic and superohmic curves and is a simple and physical analytic tool for investigating structured spectral densities with sharp features.

Before we discuss results in Sec. III we introduce our initial conditions. There are two straightforward ways of initializing a thermal SM: (i) thermalizing the SM before "activating" its interaction with the TLS and (ii) thermalizing the SM while the two subsystems are interacting. The first method can be suitably described by a thermalized distribution of Fock states of the SM. The second leads to a thermal distribution with respect to the appropriately displaced oscillator states of the SM [55]. For simplicity, we focus on the second case in the results discussed here.

III. RESULTS

Unless otherwise stated, simulations are carried out at $T = 300$ K with $J = 5$ THz, $\Omega = 100$ THz, and $\lambda = 0.05$ THz. The initial state of the system is localized at site 1, with the corresponding displaced oscillator in a thermal state, and all spectral densities have $\omega_p = 2J$, the bare TLS frequency. These parameters have been chosen to display the off-resonant SM behaviors most clearly.

We start with an ohmic SD. The effect of the bath on the TLS, with no SM present ($g = 0$), is to damp the TLS population oscillations until a thermal equilibrium steady state is reached. As can be seen in Fig. 3, this characteristic remains when increasing the SM coupling strength. There is a visible damping enhancement effect brought about as g becomes larger that is likely due to the mixing into higher energy states of the SM, which provides an increased number of decay pathways due to the broad ohmic SD. There is also

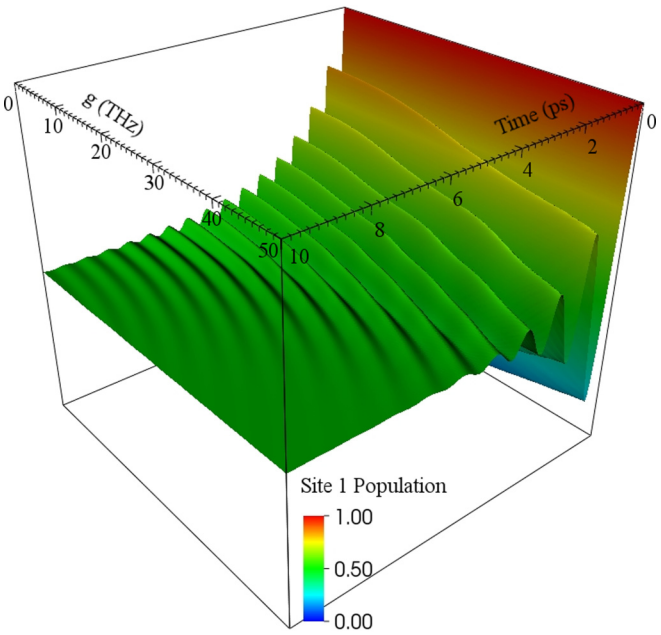

FIG. 3. Three-dimensional plot of the site 1 population dynamics as a function of g for an ohmic ($m = 1$) SD. An oscillation frequency renormalization effect is visible.

an oscillation frequency renormalization visible as a subtle curvature in the peaks as a function of g.

To further explore these effects we proceed to display the dynamics of superohmic spectral densities with $m = 3$, 5, and 7, as well as the Lorentzian SD, in Fig. 4. The qualitative difference between the dynamics in Fig. 3 and that in Fig. 4 is clear: as g is increased the oscillations are enhanced instead of damped. The behavior is most easily appreciated when looking at the second half of the simulated time in Fig. 4, where the weak-g plateaus are replaced with population oscillations for strong g. These oscillations become more pronounced with increasing m, as the SD becomes more peaked, and the largest effect is found for the Lorentzian SD, which is the most peaked of those displayed.

IV. ANALYSIS AND DISCUSSION

Without the single mode, an initial excitation at one site of the effective TLS oscillates in time between the two sites; the amplitude of this oscillation is gradually damped by the interaction with the environment. Figures 3 and 4 show that the inclusion of the single mode complicates the dynamics considerably. However, the main features can be understood using an analytical approximation for the TLS-SM system in the absence of the bath.

The adiabatic approximation of Irish *et al.* [55] provides a physically intuitive basis for the TLS-SM system in the case, as here, where the energy splitting of the TLS (here $2J = 10$ THz) is much smaller than the frequency of the SM (here $\Omega = 100$ THz). In this parameter regime the system may be approximated by two harmonic potential wells, each associated with one site of the TLS. The effect of the interaction between the SM and the TLS is to displace each harmonic well in position space. To lowest order in the TLS energy, the eigenstates of the system are given by

$$|\Psi_{\pm,n}\rangle = \frac{1}{\sqrt{2}}(|0\rangle \otimes |n_0\rangle \pm |1\rangle \otimes |n_1\rangle), \tag{21}$$

where $|i\rangle$ corresponds to excitation of site i and $|n_i\rangle$ denotes a number state of the displaced well associated with site i. Specifically, in terms of the original SM basis states $|n\rangle$ the displaced bases are given by $|n_0\rangle = \exp[-(g/\Omega)(\hat{a}^\dagger + \hat{a})]\,|n\rangle$ and $|n_1\rangle = \exp[(g/\Omega)(\hat{a}^\dagger + \hat{a})]\,|n\rangle$. The approximate energies are given by

$$E_{\pm,n} = \Omega\left(n - \frac{g^2}{\Omega^2}\right) \pm J e^{-2g^2/\Omega^2} L_n\left(\frac{4g^2}{\Omega^2}\right), \tag{22}$$

where $L_n(x)$ is a Laguerre polynomial. As shown in Fig. 5, the energy spectrum breaks into a series of well-spaced doublets, where each doublet corresponds to a different value of n.

Within this approximation, it is readily seen that an initial excitation at site i, with the SM in a number state in the displaced basis $|n_i\rangle$, will undergo Rabi-like oscillations between the two sites. The frequency of this oscillation is determined by the doublet splitting, $2Je^{-2g^2/\Omega^2}L_n(4g^2/\Omega^2)$. From this formula it is evident that one effect of increasing the coupling g is a renormalization of the oscillation frequency to smaller values, as shown in Figs. 3 and 4. Moreover, the renormalized frequency depends on the number state of the SM. Hence a distribution of different n values in the initial

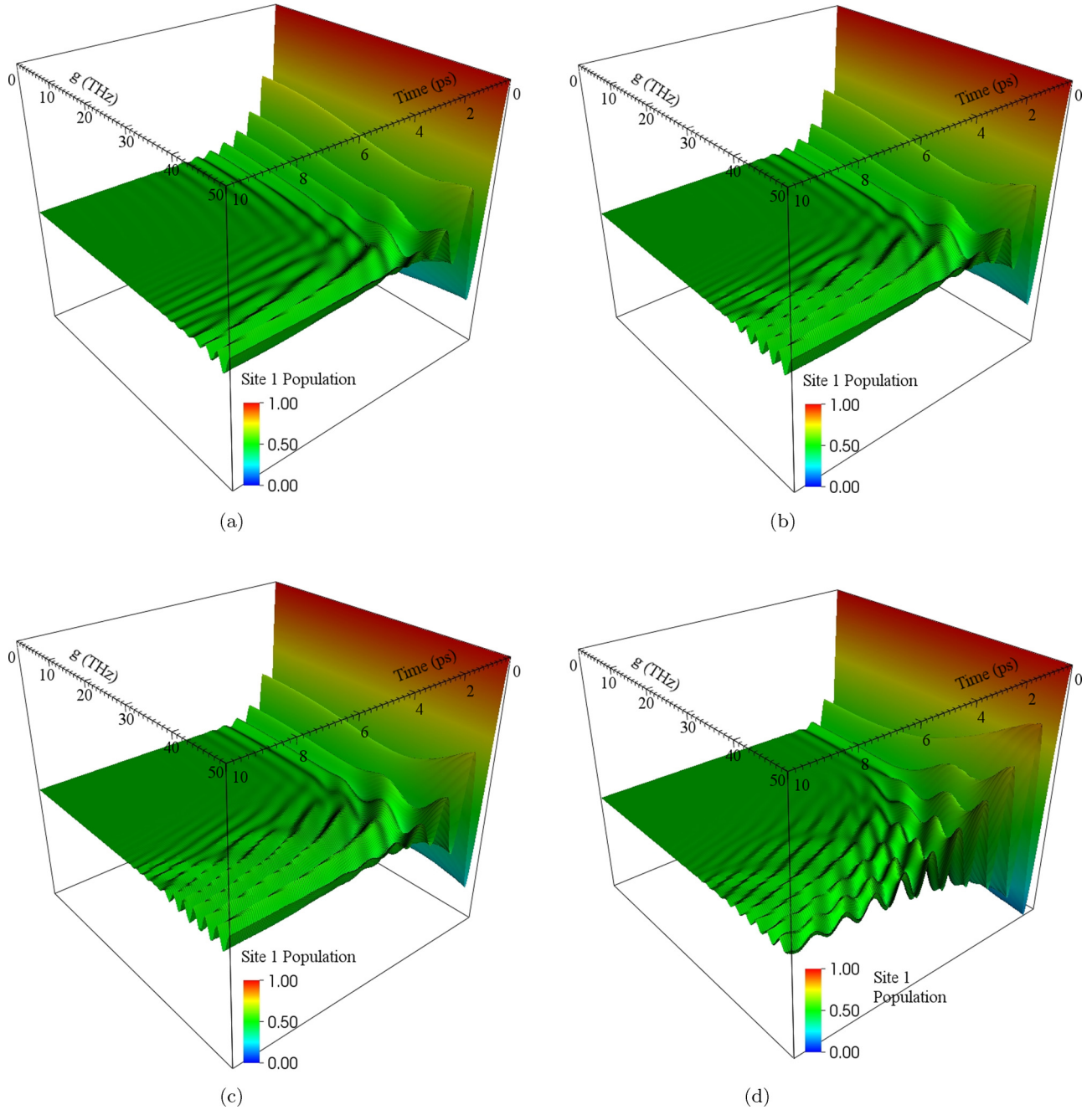

FIG. 4. Site 1 population dynamics as a function of g for superohmic spectral densities with (a) $m = 3$, (b) $m = 5$, (c) $m = 7$, and (d) Lorentzian width $W = 1.5$ THz. A clear enhancement is seen for large values of g, which becomes more pronounced for the more peaked spectral densities.

state of the SM will lead to multiple oscillation frequencies in the dynamics of the TLS population.

For the SM frequency and temperature values we consider, only two doublets contribute significantly. A thermal state of a 100-THz mode at $T = 300$ K is in the ground state with probability $p(0) \approx 92\%$, the first excited state has probability $p(1) \approx 7\%$, and all other states have a probability of less than 1%. Therefore the dynamics in Figs. 3 and 4 are dominated by just two oscillation frequencies. Figure 6(a) shows how these two frequencies change with the coupling g. Both frequencies display a strong renormalization effect, shifting to smaller values as g increases; however, the frequency corresponding to $n = 1$ changes more rapidly with g.

In addition to the frequency shift shown clearly in Fig. 3, several other aspects of the dynamics illustrated in Fig. 4 can be explained by the frequency renormalization effect. Figure 4 shows an apparently counterintuitive decrease in the damping of the oscillations as g is increased. This arises from the combination of frequency renormalization and the peaked form of the superohmic spectral densities. The spectral densities have been chosen to have their peaks at the bare oscillation frequency $2J$. As g increases, the oscillation

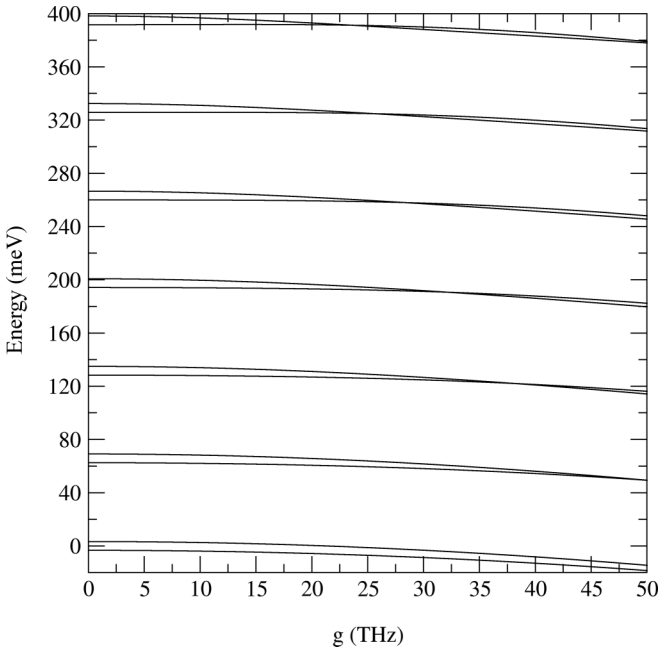

FIG. 5. Numerically determined energy spectrum of the TLS-SM system in the absence of the environment, as a function of the coupling g. Energy levels take the form of a series of closely spaced doublets.

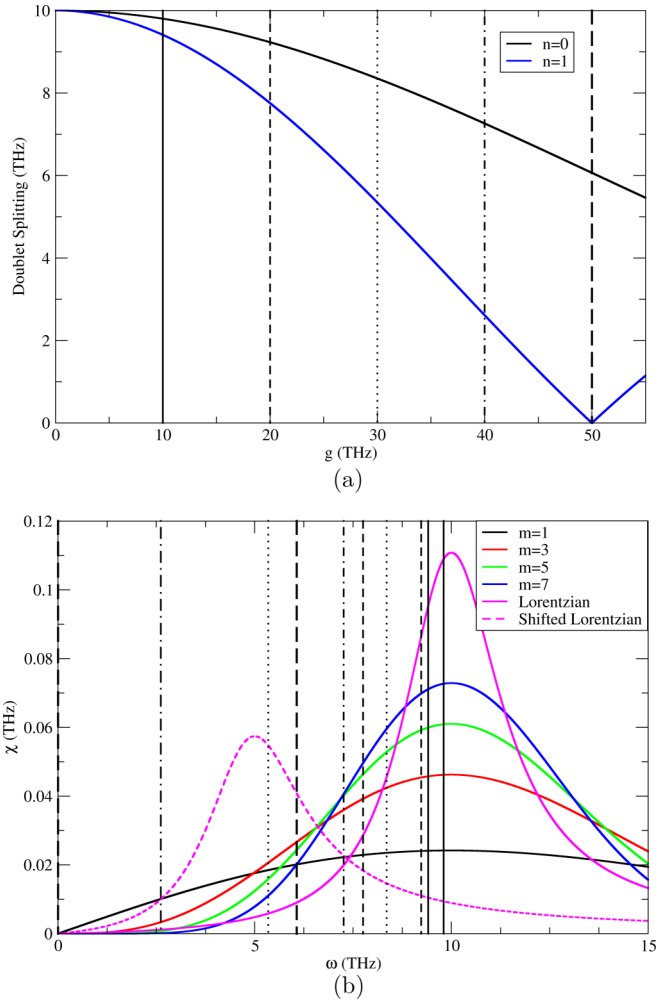

FIG. 6. (a) Energy splittings in the adiabatic approximation as a function of g, for the doublets corresponding to the $n = 0$ (black line) and $n = 1$ (blue line) states of the displaced SM. Vertical lines indicate the values of g used in (b). (b) Comparison of the doublet splittings with the various spectral densities, showing the frequencies at which the spectral densities are sampled for various values of g. Vertical lines indicate the $n = 0$ and $n = 1$ splittings for the values of g represented in (a) by the same line style. In each case the higher frequency corresponds to $n = 0$, and the lower to $n = 1$. As g increases, both frequencies decrease but they also move farther apart.

frequencies shift to lower values, moving away from the maximum of the SD. Figure 6(b) illustrates this effect for the frequencies corresponding to the $n = 0$ and $n = 1$ doublets. The vertical lines indicate the renormalized frequencies for a range of g values, showing the points at which the SD is sampled. The smaller value of $\chi(\omega)$ at lower frequencies means that the system undergoes less damping. In particular, the $n = 1$ oscillation frequency decreases more rapidly with g and thus is damped much less than the $n = 0$ mode.

In Figs. 4(a)–4(c) the oscillations that persist out to long times for large g correspond to the $n = 1$ component of the initial state, as the dominant $n = 0$ component is damped away fairly rapidly. As the SD becomes more strongly peaked, this effect becomes more pronounced, which is consistent with the trend visible in Fig. 4. The oscillations along the g axis arise from the g-dependent shift in frequency of the $n = 1$ component. By contrast, the dominant oscillation visible in Fig. 4(d) at large g values corresponds to the $n = 0$ renormalized frequency. As shown in Fig. 6(b), the Lorentzian SD at this frequency is much smaller than the ohmic or superohmic SDs and hence the $n = 0$ oscillation decays much more slowly.

In Fig. 7 we show long-time, nanosecond dynamics for the $m = 3$ superohmic SD and a very strong coupling of $g = 50$ THz. There is a very long-lived oscillatory component to the dynamics that shows no signs of decay even after 5 ns—though we have checked numerically that it does eventually reach a steady-state population of 0.5. This feature is also visible, but not so obvious, in Figs. 4(a)–4(c) through the seemingly fixed population, away from the equilibrium population of 0.5, for $t \gtrsim 6$ ps. An initial transient regime exists over a period of tens of picoseconds and can just be discerned in Fig. 7. During this transient stage other oscillatory frequencies present in the dynamics are damped away, leaving only the single slow feature associated with the $n = 1$ doublet, which, as shown in Fig. 6(a), is close to degeneracy at $g = 50$ THz. The amplitude of this persistent slow oscillation corresponds to the probability of the $n = 1$ state in the initial thermal distribution of the SM, here about 7%.

This interpretation of our results predicts that the effect of increasing g should be reversed if the peak of the SD lies at a frequency below the bare $2J$ splitting of the TLS. Then as g increases the renormalized oscillation frequencies will be pushed toward the peak of the SD rather than away from it, resulting in increased damping. In Fig. 8 we present the dynamics for such a scenario, where the peak of the Lorentzian SD is chosen to be $\omega_p = J = 5$ THz, shown as the shifted Lorentzian in Fig. 6(b). Note that the choice to keep

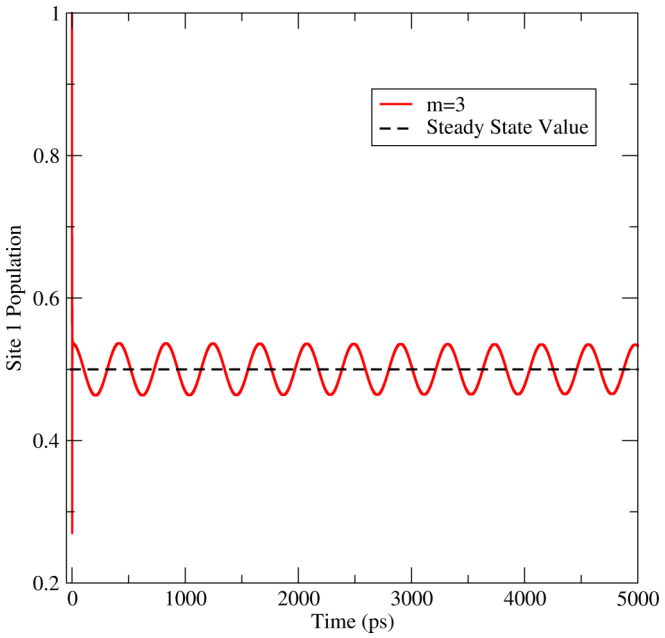

FIG. 7. An example of long-time dynamics for a strongly coupled TLS-SM system, $g = 50$ THz. The frequency and amplitude of the oscillation correspond to the $n = 1$ state of the SM. Strong frequency renormalization due to the large value of g means that the bath has an extremely weak damping effect, allowing coherent oscillations to persist out to very long times despite the influence of the environment.

the renormalization energy λ constant means that the peak height is lower than the Lorentzian centered at $\omega_p = 2J$. For values of $g \sim 40$–50 THz, the renormalized $n = 0$ frequency corresponds to a point where $\chi_L(\omega)$ is increasing rapidly; the corresponding increase in damping is dramatically evident in the dynamics.

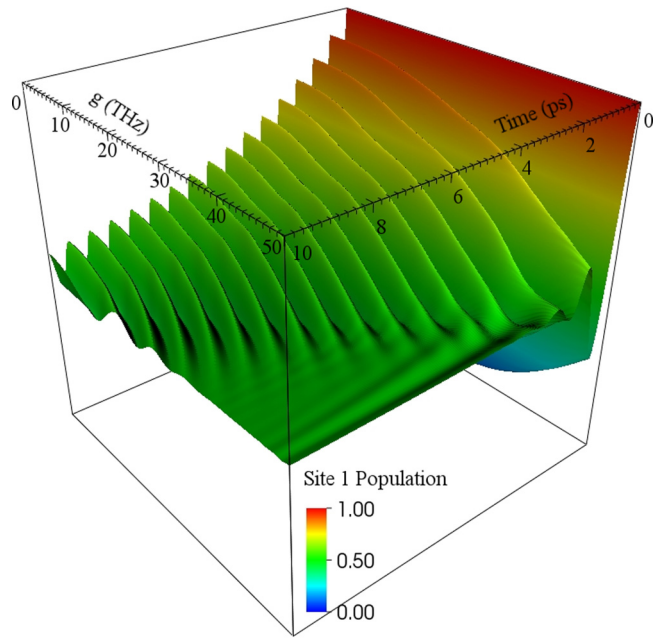

FIG. 8. Site 1 population dynamics of the TLS where the bath SD is given by a Lorentzian with peak frequency $\omega_p = J = 5$ THz. In this case increasing g pushes the oscillation frequencies of the system toward the peak of the SD rather than away from it, resulting in greater damping.

V. CONCLUSION

We have found that a single strongly coupled bosonic mode can have a profound effect on the coherent dynamics of an open TLS. Contrary to naive expectations, our work shows that strong coupling to a vibrational mode can actually enhance quantum coherent features in site-to-site dynamics. Moreover, we have shown that this effect happens for a mode that is far off-resonant with the TLS's natural oscillation frequency and that it can occur at room temperature. We have also found that certain spectral densities exhibit this coherence enhancement to differing degrees; this is a consequence of their peakedness and, so, how quickly the frequencies at which the SD is sampled are moved away from the peak by the SM coupling. We point out that some features of the results we have presented could be reproduced by including the SM as an additional strong peak in the bath SD and then using a Markovian master equation to generate the dynamics. It is vital, however, to make a polaron transform first, as might be expected when trying to describe this extra strongly coupled mode. This transformation enables the system decay rate to depend on the spectral density sampled at the coupling energy J *renormalized* by the polaronic dressing [56]. It is this renormalization that could move the position at which the spectral density is sampled when the extra mode is included. Of course, this model would not be able to capture the complex multifrequency effects we predict in this paper.

Our results show that off-resonant modes contribute to the dynamics when treated exactly, providing justification for efforts extending theoretical tools to accommodate such treatments. If an open TLS interacts with an environment with a SD like those investigated here, we have shown that its coherence properties are altered. SD modification has recently been demonstrated through reservoir engineering [18], and we speculate that using this technology with a strongly coupled vibrational mode could lead to a tool for maintaining or quickly damping oscillatory dynamics. Future work will need to generalize our approach to explore asymmetric dimers strongly coupled to more than one mode. Nonetheless, our findings provide a tantalizing look at the possibilities for novel quantum effects in complex open quantum systems.

ACKNOWLEDGMENTS

We would like to thank Ahsan Nazir and Erik Gauger for useful discussions. This work was supported by the Leverhulme Trust (RPG-080) and the EPSRC (EP/G03673X/1).

APPENDIX A: FULTON-GOUTERMAN TRANSFORMATION

The way that the FGT isolates parity subspaces can be seen if we take the Hamiltonian in Eq. (8) and transform it from the site into the superposition basis, $|\pm\rangle = \frac{1}{\sqrt{2}}(|0\rangle \pm |1\rangle)$. Writing out the matrix representation of the resulting Hamiltonian

(keeping the SM in the Fock basis) we get

$$H = \begin{array}{c} \\ \langle +0| \\ \langle -0| \\ \langle +1| \\ \langle -1| \\ \vdots \end{array} \begin{array}{c} \begin{array}{ccccc} |+0\rangle & |-0\rangle & |+1\rangle & |-1\rangle & \cdots \end{array} \\ \begin{pmatrix} -J & 0 & 0 & -h & \cdots \\ 0 & J & -h & 0 & \cdots \\ 0 & -h & -J+\Omega & 0 & \cdots \\ -h & 0 & 0 & J+\Omega & \cdots \\ \vdots & \vdots & \vdots & \vdots & \ddots \end{pmatrix} \end{array}. \tag{A1}$$

If we look at even and odd excitation parity states we see only elements linking states of like parity, meaning one can build two subspace Hamiltonians,

$$H^+ = \begin{array}{c} \\ \langle +0| \\ \langle -1| \\ \vdots \end{array} \begin{array}{c} \begin{array}{ccc} |+0\rangle & |-1\rangle & \cdots \end{array} \\ \begin{pmatrix} -J & -h & \cdots \\ -h & J+\Omega & \cdots \\ \vdots & \vdots & \ddots \end{pmatrix} \end{array},$$

$$H^- = \begin{array}{c} \\ \langle -0| \\ \langle +1| \\ \vdots \end{array} \begin{array}{c} \begin{array}{ccc} |-0\rangle & |+1\rangle & \cdots \end{array} \\ \begin{pmatrix} J & -h & \cdots \\ -h & -J+\Omega & \cdots \\ \vdots & \vdots & \ddots \end{pmatrix} \end{array}. \tag{A2}$$

In operator form these subspace Hamiltonians are the same as those in Eq. (12), which are obtained after direct application of the FGT.

APPENDIX B: INTERACTION PICTURE

The interaction picture form of our interaction Hamiltonian, $H_{\rm I}(t)$, is reached using a unitary operator approach,

$$H_{\rm I}(t) = e^{i(H_{\rm S}+H_{\rm B})t} H_{\rm I} e^{-i(H_{\rm S}+H_{\rm B})t}, \tag{B1}$$

where all of the Hamiltonians on the right-hand side are in their Schrödinger form as found in Eq. (15), with $H_{\rm B} = \sum_{\mathbf{q}} \omega_{\mathbf{q}} \hat{n}_{\mathbf{q}}$ and $H_{\rm I} = \hat{\sigma}_x \sum_{\mathbf{q}} h_{\mathbf{q}} (\hat{b}^\dagger_{\mathbf{q}} + \hat{b}_{\mathbf{q}})$. Since $[H_{\rm S}, H_{\rm B}] = 0$ and since $H_{\rm I}$ can be written in a separable form we can also formulate $H_{\rm I}(t)$ in a separable form,

$$H_{\rm I}(t) = e^{iH_{\rm S}t} \hat{\sigma}_x e^{-iH_{\rm S}t} \otimes e^{iH_{\rm B}t} \sum_{\mathbf{q}} h_{\mathbf{q}} (\hat{b}^\dagger_{\mathbf{q}} + \hat{b}_{\mathbf{q}}) e^{-iH_{\rm B}t}. \tag{B2}$$

Now the benefit of expressing $\hat{\sigma}_x$ in terms of the FGT eigenstates, $\{|\psi^\pm_k\rangle\}$, can be seen: the exponentiated $H_{\rm S}$ will simply act on its eigenstates in Eq. (B2) and be replaced with the corresponding eigenvalues (which can be found numerically).

To change its basis we first split $\hat{\sigma}_x$ into the constituent parts $\hat{\sigma}_+ = |+\rangle\langle -|$ and $\hat{\sigma}_- = |-\rangle\langle +|$, the TLS raising and lowering operators ($\hat{\sigma}_x = \hat{\sigma}_+ + \hat{\sigma}_-$). The system eigenstates in Eq. (13) exist in a Hilbert space spanning the TLS and the SM so we need

$$\hat{\sigma}_{+n} = \hat{\sigma}_+ \otimes I = \sum_n |+n\rangle\langle -n| \tag{B3}$$

and the corresponding equation for $\hat{\sigma}_{-n}$. Next we expand the eigenstates in the superposition basis: Eq. (13) becomes

$$|\psi^\pm_k\rangle = \tfrac{1}{2}[(\hat{P} \pm 1)|+\rangle - (\hat{P} \mp 1)|-\rangle]|\phi^\pm_k\rangle. \tag{B4}$$

The oscillator subspace eigenstates are expressed in a Fock basis as

$$|\phi^\pm_k\rangle = \sum_n C^\pm_{kn} |n\rangle, \tag{B5}$$

with the coefficients, $C^\pm_{kn}$, obtained after numerical solution of the eigensystem via $C^\pm_{kn} = \langle n|\phi^\pm_k\rangle$. With these definitions we can see that the $|\pm\rangle$ states pick out different parity Fock states due to their relation with $\hat{P}$ in Eq. (B4); our eigenstates become

$$|\psi^\pm_k\rangle = \sum_{\text{even } n} C^\pm_{kn} |\pm n\rangle + \sum_{\text{odd } n} C^\pm_{kn} |\mp n\rangle. \tag{B6}$$

In this form it can clearly be seen that $\langle \psi^\pm_k | \psi^\mp_{k'} \rangle = 0$ due to the orthogonal natures of the Fock and superposition states.

The change of basis of the TLS raising and lowering operators is done by calculating the overlap of the eigenstates with the operators in order to find the corresponding matrix elements:

$$\langle \psi^\pm_k | \hat{\sigma}_{+n} | \psi^\pm_{k'} \rangle = \langle \psi^\pm_k | \hat{\sigma}_{-n} | \psi^\pm_{k'} \rangle = 0, \tag{B7}$$

$$\langle \psi^\pm_k | \hat{\sigma}_{\pm n} | \psi^\mp_{k'} \rangle = \sum_{\text{even } n} C^\pm_{nk} C^\mp_{k'n}, \tag{B8}$$

$$\langle \psi^\mp_k | \hat{\sigma}_{\pm n} | \psi^\pm_{k'} \rangle = \sum_{\text{odd } n} C^\mp_{nk} C^\pm_{k'n}. \tag{B9}$$

The reversed subscripts on the first $C^\pm$ in each pair [compared with the definition in Eq. (B5)] is to be interpreted as complex conjugation, $C^\pm_{nk} = (C^\pm_{kn})^*$. Finally, our raising and lowering operators are

$$\hat{\sigma}_{\pm n} = \sum_{k,k'} \Bigg\{ \sum_{\text{even } n} C^\pm_{nk} C^\mp_{k'n} |\psi^\pm_k\rangle\langle\psi^\mp_{k'}| + \sum_{\text{odd } n} C^\mp_{nk} C^\pm_{k'n} |\psi^\mp_k\rangle\langle\psi^\pm_{k'}| \Bigg\}. \tag{B10}$$

Building the $\hat{\sigma}_{xn}$ operator removes one layer of complexity from the operators in Eq. (B10); adding them together means the even n terms are added to the odd n terms, leaving a sum over all n,

$$\hat{\sigma}_{xn} = \sum_{k,k',n} \{ C^+_{nk} C^-_{k'n} |\psi^+_k\rangle\langle\psi^-_{k'}| + C^-_{nk} C^+_{k'n} |\psi^-_k\rangle\langle\psi^+_{k'}| \}. \tag{B11}$$

We can now bring $\hat{\sigma}_{xn}$ into the interaction picture using Eq. (B2), giving

$$e^{iH_{\rm S}t} \hat{\sigma}_{xn} e^{-iH_{\rm S}t} = \sum_{k,k',n} \big\{ C^+_{nk} C^-_{k'n} e^{i\Lambda_{kk'}t} |\psi^+_k\rangle\langle\psi^-_{k'}| + C^-_{nk'} C^+_{kn} e^{-i\Lambda_{kk'}t} |\psi^-_{k'}\rangle\langle\psi^+_k| \big\}. \tag{B12}$$

Here the indices on the second element have been exchanged to allow for a common constant, $\Lambda_{kk'}$, to exist. This is comprised

of the eigenvalues of the two states contributing to the element,

$$\Lambda_{kk'} = E_k^+ - E_{k'}^-. \tag{B13}$$

The bath operator part of the separable Eq. (B2) moves into the interaction picture using the identities

$$e^{\alpha\hat{n}}\hat{b}e^{-\alpha\hat{n}} = \hat{b}e^{-\alpha}, \tag{B14}$$

$$e^{\alpha\hat{n}}\hat{b}^\dagger e^{-\alpha\hat{n}} = \hat{b}^\dagger e^{\alpha}. \tag{B15}$$

This allows us to compute Eq. (B2) and express the full interaction picture, interaction Hamiltonian as

$$H_{\rm I}^{\rm I}(t) = \sum_{k,k'} e^{i\Lambda_{kk'}t}\hat{B}^\dagger(t)\hat{\zeta}_{kk'}^+ + e^{-i\Lambda_{kk'}t}\hat{B}^\dagger(t)\hat{\zeta}_{k'k}^- + e^{i\Lambda_{kk'}t}\hat{B}(t)\hat{\zeta}_{kk'}^+ + e^{-i\Lambda_{kk'}t}\hat{B}(t)\hat{\zeta}_{k'k}^-. \tag{B16}$$

The $\hat{B}(t)$ are the interaction picture bath operators such that

$$\hat{B}(t) = \sum_{\mathbf{q}} h_{\mathbf{q}}\hat{b}_{\mathbf{q}}e^{-i\omega_{\mathbf{q}}t}. \tag{B17}$$

The $\hat{\zeta}$'s are Fulton-Gouterman state switching operators defined as

$$\hat{\zeta}_{kk'}^+ = \sum_n C_{nk}^+ C_{k'n}^- |\psi_k^+\rangle\langle\psi_{k'}^-|, \tag{B18}$$

$$\hat{\zeta}_{k'k}^- = \sum_n C_{nk'}^- C_{kn}^+ |\psi_{k'}^-\rangle\langle\psi_k^+|. \tag{B19}$$

APPENDIX C: MASTER EQUATION

Now we can proceed to evaluate the double commutator in Eq. (16), which requires combining the various operators we have discussed up until now; noting that $\hat{\zeta}_{kk'}^+\hat{\zeta}_{ll'}^+ = \hat{\zeta}_{k'k}^-\hat{\zeta}_{l'l}^- = 0$ helps to reduce the number of terms. Due to the separable nature of the formulas presented, the partial trace over the double commutator boils down to a trace over the bath operators in each additive term in the expanded commutators. This again allows for a further reduction of terms as $\langle\hat{B}(t)\hat{B}(t')\rangle = \langle\hat{B}^\dagger(t)\hat{B}^\dagger(t')\rangle = 0$, where the use of angular brackets denotes the trace over a thermal density matrix (the assumed state of the environmental bath). A multimode thermal density matrix takes the form

$$\rho_{\rm B} = N\prod_{\mathbf{p}} e^{-\beta\omega_{\mathbf{p}}\hat{n}_{\mathbf{p}}}, \tag{C1}$$

with the normalization constant

$$N = \prod_{\mathbf{p}'} 1 - e^{-\beta\omega_{\mathbf{p}'}}. \tag{C2}$$

This could also be written as $N = \prod_i N_i$, where $N_i = 1 - e^{-\beta\omega_i}$.

Now let us evaluate the nonzero bath correlation functions $\langle\hat{B}^\dagger(t)\hat{B}(t')\rangle$ and $\langle\hat{B}(t)\hat{B}^\dagger(t')\rangle$. We show how to explicitly evaluate the first of these:

$$\begin{aligned}
\langle\hat{B}^\dagger(t)\hat{B}(t')\rangle &= N\sum_{\{n\}}\langle n_0,n_1\ldots|\sum_{\mathbf{q}} h_{\mathbf{q}}\hat{a}_{\mathbf{q}}^\dagger e^{i\omega_{\mathbf{q}}t}\sum_{\mathbf{q}'} h_{\mathbf{q}'}\hat{a}_{\mathbf{q}'}e^{-i\omega_{\mathbf{q}'}t'}\prod_{\mathbf{p}} e^{-\beta\omega_{\mathbf{p}}\hat{n}_{\mathbf{p}}}|n_0,n_1\ldots\rangle \\
&= N\sum_{\{n\}}\langle n_0,n_1\ldots|\sum_{\mathbf{q}} h_{\mathbf{q}}^2\hat{n}_{\mathbf{q}}e^{i\omega_{\mathbf{q}}(t-t')}\prod_{\mathbf{p}} e^{-\beta\omega_{\mathbf{p}}\hat{n}_{\mathbf{p}}}|n_0,n_1\rangle\ldots \\
&= N\sum_{\{n\}}\langle n_0,n_1\ldots|h_0^2\hat{n}_0e^{i\omega_0(t-t')}\prod_{\mathbf{p}} e^{-\beta\omega_{\mathbf{p}}\hat{n}_{\mathbf{p}}} + h_1^2\hat{n}_1e^{i\omega_1(t-t')}\prod_{\mathbf{p}} e^{-\beta\omega_{\mathbf{p}}\hat{n}_{\mathbf{p}}} + \ldots|n_0,n_1\ldots\rangle \\
&= N\sum_{\{n\}}\left[\langle n_0,n_1\ldots|h_0^2\hat{n}_0e^{i\omega_0(t-t')}\prod_{\mathbf{p}} e^{-\beta\omega_{\mathbf{p}}\hat{n}_{\mathbf{p}}}|n_0,n_1\ldots\rangle + \langle n_0,n_1\ldots|h_1^2\hat{n}_1e^{i\omega_1(t-t')}\prod_{\mathbf{p}} e^{-\beta\omega_{\mathbf{p}}\hat{n}_{\mathbf{p}}}|n_0,n_1\ldots\rangle + \ldots\right] \\
&= \prod_i N_i\sum_{\{n\}}\left[h_0^2\hat{n}_0e^{i\omega_0(t-t')}\prod_{\mathbf{p}} e^{-\beta\omega_{\mathbf{p}}\hat{n}_{\mathbf{p}}} + h_1^2\hat{n}_1e^{i\omega_1(t-t')}\prod_{\mathbf{p}} e^{-\beta\omega_{\mathbf{p}}\hat{n}_{\mathbf{p}}} + \ldots\right].
\end{aligned} \tag{C3}$$

In the last line of Eq. (C3) each instance of the product over $\mathbf{p}$ has all of its elements cancel with the elements in the normalization product [Eq. (C2)], except when $\mathbf{p}$ equals the index of the term the product is a part of. This leads to

$$\langle\hat{B}^\dagger(t)\hat{B}(t')\rangle = \sum_{\mathbf{p}} N_{\mathbf{p}}h_{\mathbf{p}}^2e^{i\omega_{\mathbf{p}}(t-t')}\sum_{n_{\mathbf{p}}} n_{\mathbf{p}}e^{-\beta\omega_{\mathbf{p}}n_{\mathbf{p}}} = \sum_{\mathbf{p}} h_{\mathbf{p}}^2\frac{e^{i\omega_{\mathbf{p}}(t-t')}}{e^{\beta\omega_{\mathbf{p}}}-1}. \tag{C4}$$

The last step in the process of solving the partial trace involves the SD,

$$\chi(\omega) = \sum_{\mathbf{q}} |h_{\mathbf{q}}|^2\,\delta(\omega-\omega_{\mathbf{q}}), \tag{C5}$$

which uses the bath coupling factors, $h_{\mathbf{q}}$, to describe the action of the bath. Due to the delta function summation we can write the identity

$$\int d\omega\,\chi(\omega)\phi(\omega) = \int d\omega\sum_{\mathbf{k}} h_{\mathbf{k}}^2\delta(\omega-\omega_{\mathbf{k}})\phi(\omega) = \sum_{\mathbf{k}} h_{\mathbf{k}}^2\int d\omega\,\phi(\omega)\delta(\omega-\omega_{\mathbf{k}}) = \sum_{\mathbf{k}} h_{\mathbf{k}}^2\phi(\omega_{\mathbf{k}}). \tag{C6}$$

Applying this to Eq. (C4) gives, finally,

$$\langle \hat{B}^\dagger(t)\hat{B}(t')\rangle = \int d\omega\, \chi(\omega)\frac{e^{i\omega(t-t')}}{e^{\beta\omega}-1}. \tag{C7}$$

The evolution of the second bath correlation function follows similarly, using $\hat{a}\hat{a}^\dagger = \hat{n}+1$ instead of $\hat{a}^\dagger\hat{a} = \hat{n}$. This leads to

$$\langle \hat{B}(t)\hat{B}^\dagger(t')\rangle = \int d\omega\, \chi(\omega)\frac{e^{-i\omega(t-t')}}{1-e^{-\beta\omega}}. \tag{C8}$$

By employing the identity

$$\int_0^\infty ds e^{i(a-b)s} = \pi\delta(a-b) + \frac{P}{i(a-b)} \tag{C9}$$

(where we neglect the second, principle value, term, which would lead to only small Lamb shifts), the integrals over s, in Eq. (16), and ω, introduced by the bath correlation functions, can now be performed. Let us look at one of the four terms produced when expanding the double commutator present in Eq. (16):

$$\begin{aligned} H_{\rm I}^1(t)H_{\rm I}^1(t-s)\rho(t) = &\sum_{k,k',p,p'} [\langle \hat{B}^\dagger(t)\hat{B}(t-s)\rangle + \langle \hat{B}(t)\hat{B}^\dagger(t-s)\rangle] \\ &\times [e^{i(\Lambda_{kk'}-\Lambda_{pp'})t}e^{i\Lambda_{pp'}s}\hat{\zeta}^+_{kk'}\hat{\zeta}^-_{p'p}\rho_{\rm S}(t) + e^{-i(\Lambda_{kk'}-\Lambda_{pp'})t}e^{-i\Lambda_{pp'}s}\hat{\zeta}^-_{k'k}\hat{\zeta}^+_{pp'}\rho_{\rm S}(t)]. \end{aligned} \tag{C10}$$

Again, to proceed we explicitly show here one example of how to evaluate these terms, with the others being similarly computable:

$$\int_0^\infty ds\, \langle \hat{B}^\dagger(t)\hat{B}(t-s)\rangle e^{\pm i\Lambda_{pp'}s} = \int_0^\infty ds \int_0^\infty d\omega\, \chi(\omega)\frac{e^{i(\omega\pm\Lambda_{pp'})s}}{e^{\beta\omega}-1} = \int_0^\infty d\omega\, \chi(\omega)\frac{\delta(\omega\pm\Lambda_{pp'})}{e^{\beta\omega}-1} = \frac{\pi\chi(\mp\Lambda_{pp'})}{e^{\mp\beta\Lambda_{pp'}}-1} = \Gamma(\mp\Lambda_{pp'}). \tag{C11}$$

We have defined Γ (and also shortly Γ') to simplify future equations; it describes the thermal decay rate of the associated transition denoted Λ. The three remaining terms are

$$\int_0^\infty ds\, \langle \hat{B}^\dagger(t-s)\hat{B}(t)\rangle e^{\pm i\Lambda_{pp'}s} = \frac{\pi\chi(\pm\Lambda_{pp'})}{e^{\pm\beta\Lambda_{pp'}}-1} = \Gamma(\pm\Lambda_{pp'}), \tag{C12}$$

$$\int_0^\infty ds\, \langle \hat{B}(t)\hat{B}^\dagger(t-s)\rangle e^{\pm i\Lambda_{pp'}s} = \frac{\pi\chi(\pm\Lambda_{pp'})}{1-e^{\mp\beta\Lambda_{pp'}}} = \Gamma'(\pm\Lambda_{pp'}), \tag{C13}$$

$$\int_0^\infty ds\, \langle \hat{B}(t-s)\hat{B}^\dagger(t)\rangle e^{\pm i\Lambda_{pp'}s} = \frac{\pi\chi(\mp\Lambda_{pp'})}{1-e^{\pm\beta\Lambda_{pp'}}} = \Gamma'(\mp\Lambda_{pp'}). \tag{C14}$$

We are now in a position to write out the first form of the differential equation we have been working towards from Eq. (16):

$$\begin{aligned} \frac{d\rho_{\rm S}(t)}{dt} = -\sum_{k,k',p,p'} \{ &[\Gamma(-\Lambda_{pp'})+\Gamma'(\Lambda_{pp'})]e^{i(\Lambda_{kk'}-\Lambda_{pp'})t}\hat{\zeta}^+_{kk'}\hat{\zeta}^-_{p'p}\rho_{\rm S}(t) + [\Gamma(\Lambda_{pp'})+\Gamma'(-\Lambda_{pp'})]e^{-i(\Lambda_{kk'}-\Lambda_{pp'})t}\hat{\zeta}^-_{k'k}\hat{\zeta}^+_{pp'}\rho_{\rm S}(t) \\ &+ [\Gamma(-\Lambda_{kk'})+\Gamma'(\Lambda_{kk'})]e^{i(\Lambda_{kk'}-\Lambda_{pp'})t}\rho_{\rm S}(t)\hat{\zeta}^+_{kk'}\hat{\zeta}^-_{p'p} + [\Gamma(\Lambda_{kk'})+\Gamma'(-\Lambda_{kk'})]e^{-i(\Lambda_{kk'}-\Lambda_{pp'})t}\rho_{\rm S}(t)\hat{\zeta}^-_{k'k}\hat{\zeta}^+_{pp'} \\ &- [\Gamma(-\Lambda_{pp'})+\Gamma'(\Lambda_{pp'})][e^{i(\Lambda_{kk'}+\Lambda_{pp'})t}\hat{\zeta}^+_{kk'}\rho_{\rm S}(t)\hat{\zeta}^+_{pp'} + e^{-i(\Lambda_{kk'}-\Lambda_{pp'})t}\hat{\zeta}^-_{k'k}\rho_{\rm S}(t)\hat{\zeta}^+_{pp'}] \\ &- [\Gamma(\Lambda_{pp'})+\Gamma'(-\Lambda_{pp'})][e^{-i(\Lambda_{kk'}+\Lambda_{pp'})t}\hat{\zeta}^-_{k'k}\rho_{\rm S}(t)\hat{\zeta}^-_{p'p} + e^{i(\Lambda_{kk'}-\Lambda_{pp'})t}\hat{\zeta}^+_{kk'}\rho_{\rm S}(t)\hat{\zeta}^-_{p'p}] \\ &- [\Gamma(\Lambda_{kk'})+\Gamma'(-\Lambda_{kk'})][e^{i(\Lambda_{kk'}+\Lambda_{pp'})t}\hat{\zeta}^+_{kk'}\rho_{\rm S}(t)\hat{\zeta}^+_{pp'} + e^{i(\Lambda_{kk'}-\Lambda_{pp'})t}\hat{\zeta}^+_{kk'}\rho_{\rm S}(t)\hat{\zeta}^-_{p'p}] \\ &- [\Gamma(-\Lambda_{kk'})+\Gamma'(\Lambda_{kk'})][e^{-i(\Lambda_{kk'}+\Lambda_{pp'})t}\hat{\zeta}^-_{k'k}\rho_{\rm S}(t)\hat{\zeta}^-_{p'p} + e^{-i(\Lambda_{kk'}-\Lambda_{pp'})t}\hat{\zeta}^-_{k'k}\rho_{\rm S}(t)\hat{\zeta}^+_{pp'}]\}. \end{aligned} \tag{C15}$$

In order to simplify Eq. (C15) we employ the secular approximation, which assumes that if the oscillatory exponential factors have a nonzero frequency (i.e., $\Lambda_{kk'}-\Lambda_{pp'} \neq 0 \neq \Lambda_{kk'}+\Lambda_{pp'}$), then they correspond to a rapid oscillation compared to the time scale over which we have assumed the system density matrix changes. These terms are neglected. To ensure $\Lambda_{kk'}-\Lambda_{pp'}=0$ we can insert $\delta_{k,q}\delta_{k',q'}$ into the summation. Now $\Lambda_{kk'}+\Lambda_{pp'} \to 2\Lambda_{kk'}$, which in general is nonzero, so these terms are neglected also [the special case of $2\Lambda_{kk}=0$ would similarly mean $\Gamma(\pm\Lambda_{kk})=0$ and thus would not contribute to the dynamics]. Equation (C15) can now be written in Lindblad form, thus we obtain the stated result in Eq. (17).

[1] G. S. Engel, T. R. Calhoun, E. L. Read, T.-K. Ahn, T. Mancal, Y.-C. Cheng, R. E. Blankenship, and G. R. Fleming, Nature **446**, 782 (2007).

[2] A. W. Chin, S. F. Huelga, and M. B. Plenio, Phys. Rev. Lett. **109**, 233601 (2012).

[3] T. J. G. Apollaro, C. Di Franco, F. Plastina, and M. Paternostro, Phys. Rev. A **83**, 032103 (2011).

[4] B.-H. Liu, L. Li, Y.-F. Huang, C.-F. Li, G.-C. Guo, E.-M. Laine, H.-P. Breuer, and J. Piilo, Nat. Phys. **7**, 931 (2011).

[5] G. Ritschel, J. Roden, W. T. Strunz, and A. Eisfeld, New J. Phys. **13**, 113034 (2011).

[6] C. Kreisbeck and T. Kramer, J. Phys. Chem. Lett. **3**, 2828 (2012).

[7] M. del Rey, A. W. Chin, S. F. Huelga, and M. B. Plenio, J. Phys. Chem. Lett. **4**, 903 (2013).

[8] A. W. Chin, J. Prior, R. Rosenbach, F. Caycedo-Soler, S. F. Huelga, and M. B. Plenio, Nat. Phys. **9**, 113 (2013).

[9] E. K. Irish, R. Gómez-Bombarelli, and B. W. Lovett, Phys. Rev. A **90**, 012510 (2014).

[10] N. Killoran, S. F. Huelga, and M. B. Plenio, J. Chem. Phys. **143**, 155102 (2015).

[11] A. G. Dijkstra, C. Wang, J. Cao, and G. R. Fleming, J. Phys. Chem. Lett. **6**, 627 (2015).

[12] P. Nalbach, C. A. Mujica-Martinez, and M. Thorwart, Phys. Rev. E **91**, 022706 (2015).

[13] F. D. Fuller, J. Pan, A. Gelzinis, V. Butkus, S. S. Senlik, D. E. Wilcox, C. F. Yocum, L. Valkunas, D. Abramavicius, and J. P. Ogilvie, Nat. Chem. **6**, 706 (2014).

[14] E. Romero, R. Augulis, V. I. Novoderezhkin, M. Ferretti, J. Thieme, D. Zigmantas, and R. van Grondelle, Nat. Phys. **10**, 676 (2014).

[15] J. Lim, D. Palecek, F. Caycedo-Soler, C. N. Lincoln, J. Prior, H. von Berlepsch, S. F. Huelga, M. B. Plenio, D. Zigmantas, and J. Hauer, Nat. Commun. **6**, 7755 (2015).

[16] F. Novelli, A. Nazir, G. H. Richards, A. Roozbeh, K. E. Wilk, P. M. G. Curmi, and J. A. Davis, J. Phys. Chem. Lett. **6**, 4573 (2015).

[17] S. Gröblacher, A. Trubarov, N. Prigge, G. D. Cole, M. Aspelmeyer, and J. Eisert, Nat. Commun. **6**, 7606 (2015).

[18] M. Haeberlein, F. Deppe, A. Kurcz, J. Goetz, A. Baust, P. Eder, K. Fedorov, M. Fischer, E. P. Menzel, M. J. Schwarz, F. Wulschner, E. Xie, L. Zhong, E. Solano, A. Marx, J.-J. García-Ripoll, and R. Gross, arXiv:1506.09114 [cond-mat.mes-hall].

[19] H. Breuer and F. Petruccione, *The Theory of Open Quantum Systems* (Oxford University Press, Oxford, UK, 2007).

[20] N. Makri and D. E. Makarov, J. Chem. Phys. **102**, 4600 (1995).

[21] N. Makri and D. E. Makarov, J. Chem. Phys. **102**, 4611 (1995).

[22] J. Dalibard, Y. Castin, and K. Mølmer, Phys. Rev. Lett. **68**, 580 (1992).

[23] C. H. Mak and R. Egger, Phys. Rev. E **49**, 1997 (1994).

[24] Y. Tanimura and R. Kubo, J. Phys. Soc. Jpn. **58**, 101 (1989).

[25] H. Wang, J. Phys. Chem. A **119**, 7951 (2015).

[26] M. Beck, A. Jäckle, G. Worth, and H.-D. Meyer, Phys. Rep. **324**, 1 (2000).

[27] F. B. Anders and A. Schiller, Phys. Rev. Lett. **95**, 196801 (2005).

[28] J. Prior, A. W. Chin, S. F. Huelga, and M. B. Plenio, Phys. Rev. Lett. **105**, 050404 (2010).

[29] F. A. Y. N. Schröder and A. W. Chin, Phys. Rev. B **93**, 075105 (2016).

[30] N. Zhou, Z. Huang, J. Zhu, V. Chernyak, and Y. Zhao, J. Chem. Phys. **143**, 014113 (2015).

[31] S. Bera, N. Gheeraert, S. Fratini, S. Ciuchi, and S. Florens, Phys. Rev. B **91**, 041107 (2015).

[32] A. Kolli, E. J. O'Reilly, G. D. Scholes, and A. Olaya-Castro, J. Chem. Phys. **137**, 174109 (2012).

[33] A. D. O'Connell, M. Hofheinz, M. Ansmann, R. C. Bialczak, M. Lenander, E. Lucero, M. Neeley, D. Sank, H. Wang, M. Weides, J. Wenner, J. M. Martinis, and A. N. Cleland, Nature **464**, 697 (2010).

[34] A. Wallraff, D. I. Schuster, A. Blais, L. Frunzio, R.-S. Huang, J. Majer, S. Kumar, S. M. Girvin, and R. J. Schoelkopf, Nature **431**, 162 (2004).

[35] M. Thorwart, E. Paladino, and M. Grifoni, Chem. Phys. **296**, 333 (2004).

[36] F. Brito and A. O. Caldeira, New J. Phys. **10**, 115014 (2008).

[37] J. Hausinger and M. Grifoni, New J. Phys. **10**, 115015 (2008).

[38] C. Gan, P. Huang, and H. Zheng, J. Phys.: Condens. Matter **22**, 115301 (2010).

[39] J. Iles-Smith, N. Lambert, and A. Nazir, Phys. Rev. A **90**, 032114 (2014).

[40] H. Hossein-Nejad and G. D. Scholes, New J. Phys. **12**, 065045 (2010).

[41] H. Hossein-Nejad, V. V. Albert, E. J. O'Reilly, and G. D. Scholes, New J. Phys. **16**, 019502 (2014).

[42] H.-B. Chen, J.-Y. Lien, C.-C. Hwang, and Y.-N. Chen, Phys. Rev. E **89**, 042147 (2014).

[43] U. Weiss, *Quantum Dissipative Systems.Series in Modern Condensed Matter Physics* (World Scientific, Singapore, 2008).

[44] A. J. Leggett, S. Chakravarty, A. T. Dorsey, M. P. A. Fisher, A. Garg, and W. Zwerger, Rev. Mod. Phys. **59**, 1 (1987).

[45] F. Wilhelm, S. Kleff, and J. von Delft, Chem. Phys. **296**, 345 (2004).

[46] H. Wang and M. Thoss, New J. Phys. **10**, 115005 (2008).

[47] A. Ishizaki and G. R. Fleming, J. Chem. Phys. **130**, 234111 (2009).

[48] Y. Yao, L. Duan, Z. Lü, C.-Q. Wu, and Y. Zhao, Phys. Rev. E **88**, 023303 (2013).

[49] R. L. Fulton and M. Gouterman, J. Chem. Phys. **35**, 1059 (1961).

[50] M. Wagner, J. Phys. A: Math. Gen. **17**, 3409 (1984).

[51] S. Paganelli and S. Ciuchi, J. Phys.: Condens. Matter **18**, 7669 (2006).

[52] J. Johansson, P. Nation, and F. Nori, Comput. Phys. Commun. **184**, 1234 (2013).

[53] D. P. S. McCutcheon and A. Nazir, J. Chem. Phys. **135**, 114501 (2011).

[54] A. A. Louis and J. P. Sethna, Phys. Rev. Lett. **74**, 1363 (1995).

[55] E. K. Irish, J. Gea-Banacloche, I. Martin, and K. C. Schwab, Phys. Rev. B **72**, 195410 (2005).

[56] D. P. S. McCutcheon and A. Nazir, New J. Phys. **12**, 113042 (2010).